Supporting Information for

Influence of Amorphous Carbon Interlayers on Nucleation and Early Growth of Lithium Metal at the Current Collector-Solid Electrolyte Interface

Moritz H. Futscher[1,‡,], Thomas Amelal[2,‡], Jordi Sastre[1], André Müller[1], Jyotish Patidar[2], Abdessalem Aribia[1], Kerstin Thorwarth[2], Sebastian Siol[2] and Yaroslav E. Romanyuk[1]*

[1] Laboratory for Thin Films and Photovoltaics, Empa - Swiss Federal Laboratories for Materials Science and Technology, Überlandstrasse 129, 8600 Dübendorf, Switzerland

[2] Laboratory for Surface Science and Coating Technologies, Empa - Swiss Federal Laboratories for Materials Science and Technology, Überlandstrasse 129, 8600 Dübendorf, Switzerland

[*] Corresponding author

[‡] These authors contributed equally to this work

S1 Discharge capacity

Figure S1 shows the cell voltage vs specific capacity of the different carbon films between 0.0 and 0.3 V against Li/Li^+. Due to the irreversible capacity of the first cycle, it was omitted (see Figure 3f in the main text for the change in irreversible capacity during cycling). The discharge capacity plotted in Figure 2b is the mean of the first 5 cycles.

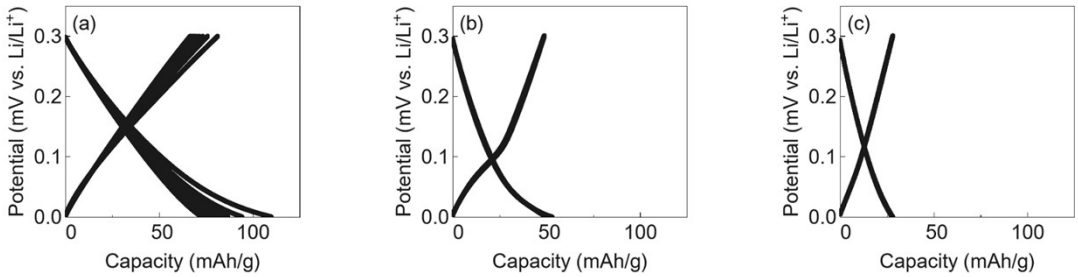

Figure S1. Voltage vs capacity of carbon films deposited **(a)** without heating, **(b)** at 250 °C, and **(c)** at 350 °C with a thickness of 100 nm.

S2 Ionic conductivity

Figure S2 shows impedance spectroscopy measurements of the different carbon films measured at 0.1 V against Li/Li^+, along with the equivalent circuit used to fit the data. We observe two semicircles and a rise at low frequency due to interfacial polarization. The interfacial polarization is described by a Warburg element (W). The semicircle at high frequencies (left) corresponds to the ionic resistance of the Lipon solid electrolyte and is described by a resistor (R1) in parallel with a constant phase element (CPE1). The second semicircle is due to the ionic resistance of the carbon layer and is described by a resistor (R2) in parallel with a constant phase element (CPE2). R0 refers to the series resistance due to contact resistances. The obtained fits are shown as red lines in Figure S2. The obtained resistance of the carbon layer is used to quantify the ionic conductivity, which is shown in Figure 2d in the main text.

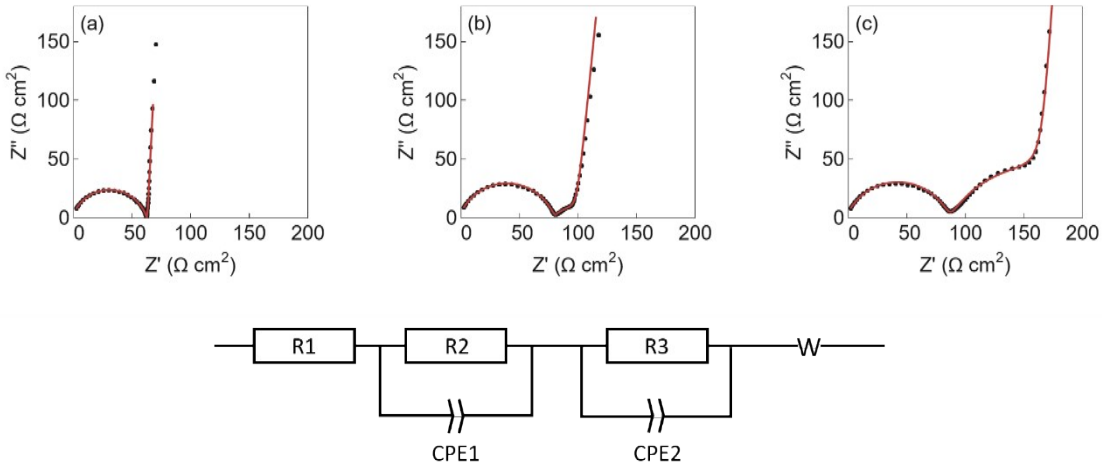

Figure S2. Impedance spectroscopy measurements performed at 0.1 V against Li/Li^+ of carbon films deposited **(a)** without heating, **(b)** at 250 °C, and **(c)** at 350 °C with a thickness of 100 nm. The equivalent circuit used to fit the impedance spectroscopy measurements is shown on the bottom. The data are shown as black dots and the obtained fits as red lines.

In addition to the increase in ionic resistance of the carbon layer, we also observe an increase in the resistance of the semicircle corresponding to the Lipon solid electrolyte from 64 to 89 $\Omega \cdot cm^2$ for carbon films deposited without heating and at 350 °C, respectively. We attribute this increase in resistance to an increase in the roughness of both the copper substrate and the carbon layer deposited at elevated temperatures, as shown in Figure 1 in the main text and in Figure S3.

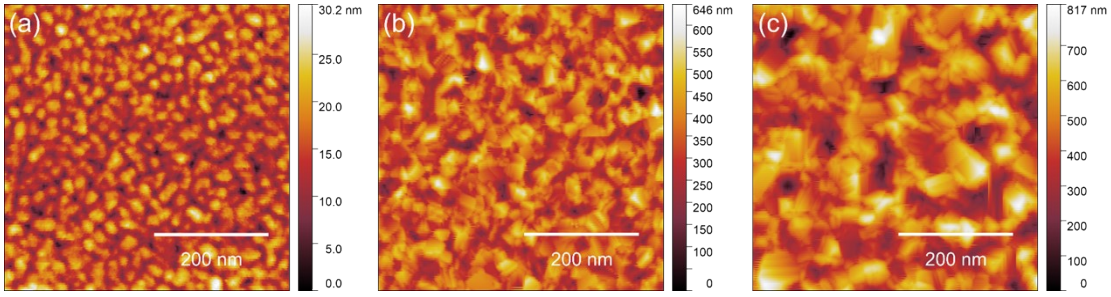

Figure S3. Atomic force microscope micrographs of copper films deposited **(a)** without heating, **(b)** at 250 °C, and **(c)** at 350 °C. The root mean square roughness of the films shown in (a), (b), and (c) is 4, 78, and 120 nm, respectively.

S3 Overpotential

Figure S4 shows a detailed view of the observed overpotential for different carbon interlayers with a thickness of 100 nm. For both the carbon film deposited without heating and the carbon film deposited at 250 °C, the voltage dip occurs only at an equivalent Li metal thickness close

to the film thickness. In contrast, for the carbon film deposited at 350 °C, the voltage dip occurs at very low equivalent Li metal thicknesses. Therefore, we assume that only the carbon films deposited without heating and at 250 °C are involved in the interphase formation. The reason why the carbon films deposited at 350 °C do not participate in the interphase formation might be related to the fractures of the layers visible in Figure 1f in the main text.

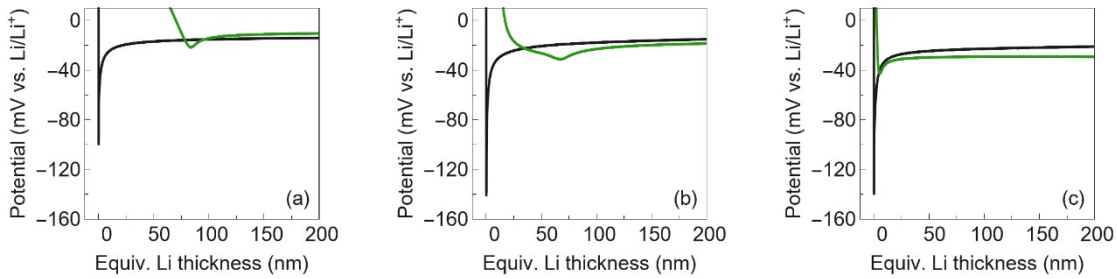

Figure S4. Plating of Li between the current collector and the solid electrolyte at a current density of 0.2 mA·cm^{-2} for carbon films deposited **(a)** without heating, **(b)** at 250 °C, and at **(c)** 350 °C with a thickness of 100 nm shown in green. The black curves correspond to the plating profiles without carbon.

Figure S5 shows a detailed view of the observed overpotential for the carbon interlayer deposited at 150 nm showing two voltage dips. We attribute the first voltage dip to the deposition of Li directly on copper, favored by the low ionic conductivity of the carbon films deposited at 350 °C, and to the fractures of the films visible in Figure 1f in the main text.

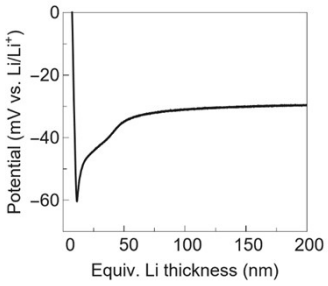

Figure S5. Plating of Li between the current collector and the solid electrolyte at a current density of 0.2 mA·cm^{-2} for a carbon film deposited at 350 °C with a thickness of 150 nm.

S4 Cross-sectional SEM micrographs

Figure S6 shows cross-sectional SEM micrographs of plated and stripped Li metal with and without a 100 nm carbon interlayer between current collector and solid electrolyte. In the case with the carbon interlayer, a dense and uniform Li metal is formed upon plating. In contrast, in the case without carbon, the Li metal is deposited very non-homogeneously. This

non-homogeneous growth of Li can lead to current focusing, which eventually can results in the formation of dendrites. This difference in the growth of the Li metal thus can explains the improvement in critical current density when a thin carbon interlayer is used. When stripping, we find that in both cases, with and without carbon, all the previously deposited Li metal is removed.

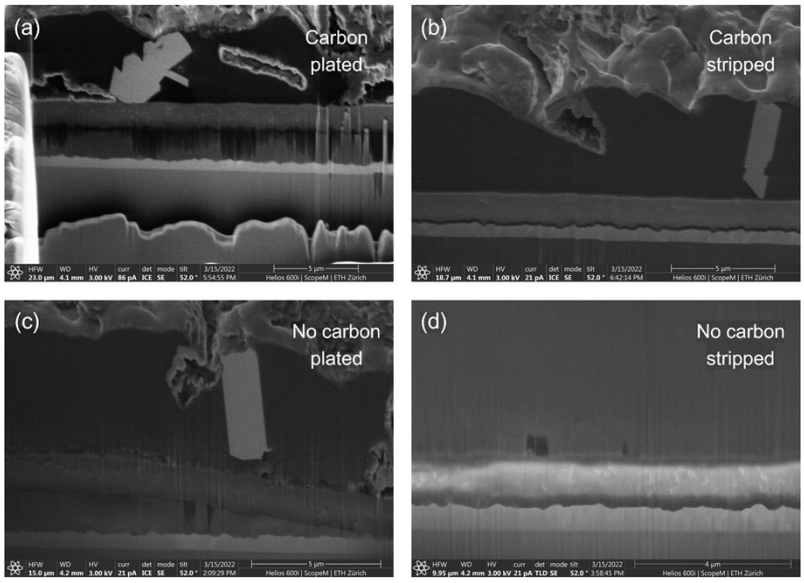

Figure S6. Cross-sectional SEM micrographs of the current collector-solid electrolyte interface with and without carbon interlayer. (a) After plating an equivalent Li thickness of 1 µm with carbon interlayer, (b) after subsequent stripping the plated Li with carbon interlayer, (c) after plating an equivalent Li thickness of 1 µm without carbon interlayer, and (d) after subsequent stripping the plated Li without carbon interlayer. The thickness of the amorphous carbon layer is 100 nm deposited at 250 °C. Plating and stripping of Li was performed at a current density of 0.2 $mA \cdot cm^{-2}$. Magnified cross-sectional SEM micrographs of (a) and (b) are shown in Figure 5 in the main text.

S5 Anode-free thin-film solid-state battery

We fabricate anode-free thin-film batteries composed of Cu/C/Lipon/LCO/Au. 250 nm of LCO was deposited via RF magnetron sputtering of a 2'' target of $LiCoO_2$ in an Orion sputtering system (AJA International Inc.) in O_2 atmosphere at a power of 100 W and a working pressure of $3 \cdot 10^{-3}$ mbar at a working distance of approximately 13 cm through a shadow mask with a diameter of 0.1 cm. 100 nm of Au was subsequently deposited by thermal evaporation through the same shadow mask. Note that the LCO did not undergo a heating treatment after deposition so as not to impair the properties of the amorphous carbon interlayers, resulting in a low capacity of the cells.

Figure S7a shows the voltage curves of the anode-free batteries with carbon interlayers of different thicknesses deposited at 250 °C. Figure S7b shows the discharge capacity as a function of C rate for the different carbon interlayers, from 3.4 (C/5) to 100.6 $\mu A \cdot cm^{-2}$ (6C). We find that carbon layers with thickness of 20 and 60 nm improve the performance compared to the reference cell without carbon. Similar to the results of the critical current density as a function of carbon thickness (Figure 4 in the main text), we find that carbon layers with thickness of 90 nm decrease the performance of the anode-free battery, which may be related to the ionic conductivity. Figure S7c shows anode-free batteries operated at a current density of 8.4 $\mu A \cdot cm^{-2}$ (C/2) for 200 cycles. While both cells show rapid capacity fading, we note that the capacity fading is less for the cells with the intermediate carbon layer than for the cells without. The difference between the cells can be attributed to the improved plating and stripping of the Li metal anode during charging and discharging.

Note that the C-rates are calculated assuming a capacity of 140 $mAh \cdot g^{-1}$ for LCO. Since the actual capacity of the as-deposited LCO is much lower (<20 $mAh \cdot g^{-1}$), actual C-rates are higher by a factor of about 7.

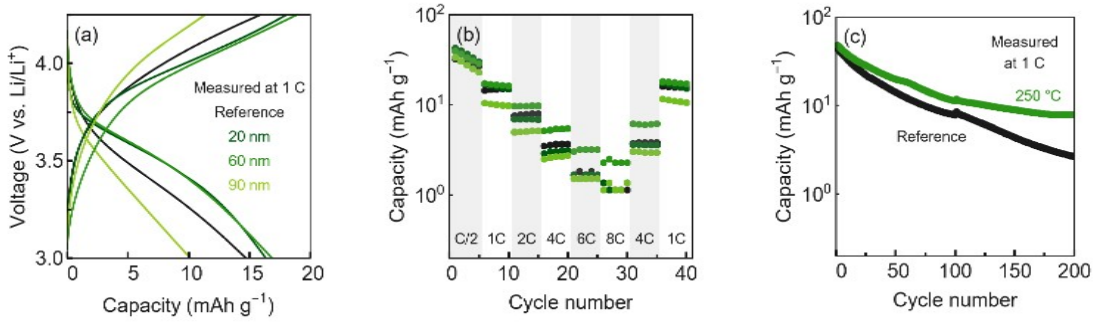

Figure S7. (a) Charge–discharge curves measured at C/2 (8.4 $\mu A \cdot cm^{-2}$) of carbon films with thicknesses ranging from 0 to 90 nm. (b) Discharge capacity of the anode-free batteries at different C rates. (c) Long-term cycling of

the battery with a carbon interlayer with a thickness 60 nm over 200 cycles at C/2 compared to a battery without carbon interlayer. All carbon thin films were deposited at 250 °C.

Figure S8a shows the voltage curves of the anode-free batteries with carbon interlayers deposited at different temperatures. Figure S8b shows the discharge capacity as a function of C rate for the different carbon interlayers, from 3.4 (C/5) to 100.6 μA·cm^{-2} (6C). We find that, while the critical current density and the overpotential of these films are comparable (see Figure 4 in the main text), the performance of the carbon film deposited at 250 °C is superior compared to the carbon films deposited without heating and at 350 °C. We thus suspect that the irreversible capacity loss, observed in the carbon films without heating, has negative implications on the performance of anode-free batteries, and that the interphase formation observed for the films deposited at 250 °C, but not at the ones deposited at 350 °C (see Figure 4 in the main text), is beneficial for the performance of anode-free batteries.

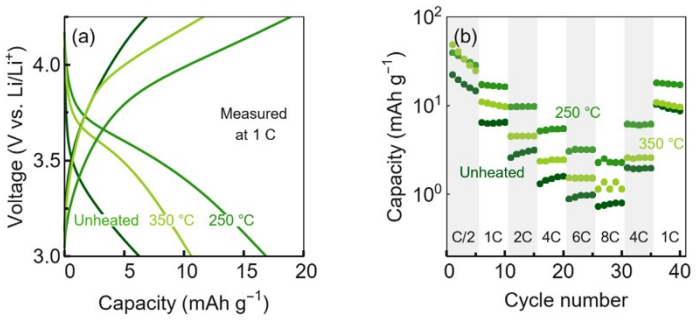

Figure S8. (a) Charge–discharge curves measured at C/2 (8.4 μA·cm^{-2}) of carbon films deposited without heating, at 250 °C, and at 350 °C. (b) Discharge capacity of the anode-free batteries at different C rates. All carbon thin films had a thickness of 60 nm.

S6 ERDA measurements

Rutherford backscattering spectrometry with 2 MeV He ions and elastic recoil detection analysis with 13 MeV 127I ions were performed at the Laboratory of Ion Beam Physics at ETH Zurich to determine the area density and composition of the carbon thin films on Si substrates. Figure S9 shows the composition of the carbon thin films for different deposition temperatures. The hydrogen can come from the background pressure of the chamber.

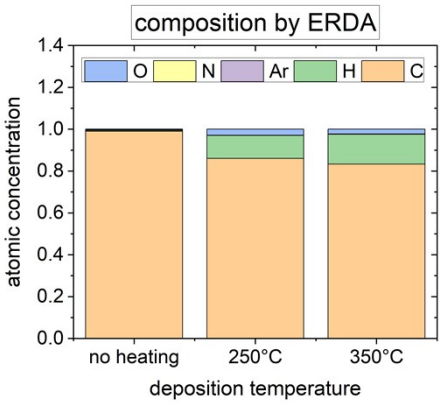

Figure S9. Composition of the carbon thin films deposited without heating, 250 °C, and 350 °C obtained by ERDA.